

Influence of Structural, Thermoelectric Power and Catalytic Efficiency of Nd-Doped Mn₃O₄

V.T. GEETHA^{1,2,*}, G. PUTHILIBAI^{1,2} and S. INDUJA¹

¹Department of Chemistry, Hindustan Institute of Technology and Science, No. 1, Rajiv Gandhi Salai (OMR), Padur, Chennai-603103, India

²Department of Chemistry, Sri Sairam Engineering College, Sai Leo Nagar, West Tambaram, Chennai-600044, India

*Corresponding author: E-mail: geethavt@yahoo.com

Received: 5 August 2019;

Accepted: 19 September 2019;

Published online: 18 November 2019;

AJC-19689

Hexagonal shape Nd doped Mn₃O₄ samples were prepared *via* microwave route using urea as reducing agent. Nd doped Mn₃O₄ magnetic, structural, optical and morphological properties of the synthesized hexagonal like particles were examined by diffused reflectance spectroscopy (DRS) and photoluminescence (PL), XRD, SEM, TEM and vibrating sample measurements (VSM) studies. Morphological results showed the hexagonal shape morphology and uniform size dispersal. The crystallite size and the particle size calculated and the TEM monographs designate the correlation of the data obtained from both measurements. It could be noted that saturation magnetization (M_s) and remanence (M_r) values reduce by maximizing neodymium replacement.

Keywords: Combustion method, Magnetic properties, Neodymium, Mn₃O₄.

INTRODUCTION

Transition metal oxides having nanometer size revealed excellent optical, electric, magnetic and catalytic attribute, when compared to bulk materials [1]. Magnetized features of nanoparticles possess numerous technological applications such as, biomedicine, drug targeting, medical imaging, catalysis, ferro-fluids and the magnetic data storage [2-4]. Consequently, dimensions of crystal, structure, morphology and surface area of oxide semiconductors may play a role that will influence the optical properties. Spinel oxides have witnessed consideration throughout the world because their unique structure, shape and the properties create a great impact in reference to the physical as well as chemical properties if their size decreased towards the nanometer scale. At present, it is a known fact in which any change in controlled morphology could possibly have significant impact on the chemical as well as physical properties of metal oxides. In connection with this, a wide range of transition metals tend to be utilized towards doping rare earth metals. Although substantial amount of work is carried out on nano-structured oxides doping, however, yet generating excellent crystalline oxides alongside interesting properties is a challenge. Neodymium are extremely worthwhile because of its distinctive qualities. Neodymium is the

most successful element among rare earth elements, due to its catalytic and optical properties and could easily be incorporated throughout Mn₃O₄ by exchanging of Mn³⁺ atom [5-7].

Doping in neodymium with a suitable dopant can make it more efficient. For example, if made magnetic on doping, neodymium doped Mn₃O₄ will become a kind of multifunctional material with magnetic, optical, semiconducting, catalytic and photocatalytic properties. Recent studies have established that acquaintance of the outer/inner surfaces of nanostructures will offer larger reactive sites, which is very critical for their catalytic performance [8,9]. The porous nanostructure is a more open nanostructure that possesses a high surface-to-volume ratio, making Nd doped Mn₃O₄ nanoparticles suitable candidates for use as catalysis [10,11].

Neodymium doped Mn₃O₄ depends on the amount of catalyst, oxidant, temperature, time, solvents, catalytic activity, surface area and magnetic properties, since Nd doped materials are affected due to change in the angles, orientations of magnetic moments change and leads to the generation of an electron e-hole pair. It has been observed that the surface area plays a major role in among all factors in the catalytic oxidation from benzyl alcohol by providing a higher surface area, which leads to the higher adsorption of aromatic alcohol to aldehyde molecule on the surface of catalyst and enhances the catalytic activity [12,13].

Different ways for the synthesis techniques were applied for manganese oxide, such as for instance, hydrothermal, sol-gel, co-precipitation, solvothermal, microwave, combustion methods and thermal decomposition [14,15]. Related to more techniques, microwave route applies the advantages of effective control on stoichiometric ratio, excellent homogeneousness, yielding thin films and powders of nanomaterials, in addition to lower handling temperature. Other techniques will cause sharp thermal gradients throughout the bulk solution and it is inefficient because of the non-uniform reaction conditions, thus leading to the high reaction temperature or long reaction time. In addition, non-uniform reaction conditions will introduce the impurities into the final products and affect the uniform nucleation and growth rate of nanomaterials [16]. Recently, the use of microwave energy as a heating source for the combustion reaction has been employed, due to its fast reaction kinetics, cleanliness and efficiency, as well as economic aspects of the process in terms of energy and time [17].

In the present research study, an effort is made for Mn_3O_4 nanopowders characterization through addition of rare earth element for instance, neodymium as dopant by effective and economical microwave method. Since, presence of different types of oxygen defects such as oxygen vacancies and interstitial oxygen in Nd doped oxides nanocrystals result in changes in their photoluminescence (PL) and catalytic properties. The objective of the present investigation is to examine the effects of magnetic properties and the performance in catalytic activity of Nd doped Mn_3O_4 .

EXPERIMENTAL

Synthesis: In a typical procedure, 6.0 mL of MnCl_2 solution (0.4 M) is added to 8.0 mL of urea (0.6 M) solution carefully under continuous stirring followed by the addition of Nd(III) solution with different concentration. The manganese precursor substance together with urea were placed inside a home based convection microwave oven (Brand: IFB, Model-20SC2) then subjected to microwave energy for 10 min at 1200 W and microwave frequency of 2450 MHz. The homogeneous mixture started to boil then evaporation takes place together with evolution of gases at the time of microwave combustion. If the mixture of chemical source is extended to automatic combustion stage, mixture gets evaporated and a solid is formed. The obtained solid was washed properly using ethanol and dried at 80 °C for 1 h. Finally the samples marked as Mn_3O_4 (a) Nd doped 0.01 (b), 0.02 (c) and 0.03 (d).

Characterization: X-ray diffraction patterns of doped and undoped Mn_3O_4 samples have been recorded by X-ray diffractometer from Rigaku by using $\text{CuK}\alpha$ radiation. High resolution scanning electron microscopy (HR-SEM) pictures have been acquired from Philips XL30 ESEM fitted alongside energy dispersive X-ray spectroscopy. High resolution transmission electron microscopy (HR-TEM) pictures were recorded on Philips EM 208 transmission electron microscope using 200 kV accelerating voltage. UV-visible spectrophotometer (Cary100) and Cary Eclipse fluorescence spectrophotometer was employed to record diffuse reflectance spectra and optical properties for as-synthesized Mn_3O_4 nanomaterials.

RESULTS AND DISCUSSION

XRD analysis: Fig. 1 depicts a typical XRD patterns of prepared Nd doped (0.01, 0.02 and 0.03 %) Mn_3O_4 nanopowders. It is noticed that single-phase sample formation of Mn_3O_4 is found. The obtained results are well harmonized with standard JCPDS card No. 80-1916. From the XRD spectra, it is observed that there are no other peaks related to the secondary phase formation of Nd doped Mn_3O_4 samples. From XRD pattern, there is a small shift in peak positions of Nd doped Mn_3O_4 nanorods towards larger angles, indicating a slight distortion in the symmetry of system due to the creation of vacancies and defects in the system. In addition, doping of Nd shows no additional peaks which conforms the incorporation of Nd^{3+} ions into Mn sites because the atomic radius of Nd^{3+} is higher than Mn^{3+} sites. The ionic radius of Mn^{3+} is smaller than that of Nd^{3+} , which leads to decrease in crystallite size for Nd doped Mn_3O_4 . The crystallite size decreases due to doping of Nd, which resulted an increase in full width at half maximum (FWHM) value [18,19]. In this work, the results were found to be 71.132, 70.231, 69.209 and 70.109 Å³ for pure Mn_3O_4 and Nd doped Mn_3O_4 nanopowders, respectively. Moreover, the unit cell volumes decreased due to the doping effect of the rare metal ions.

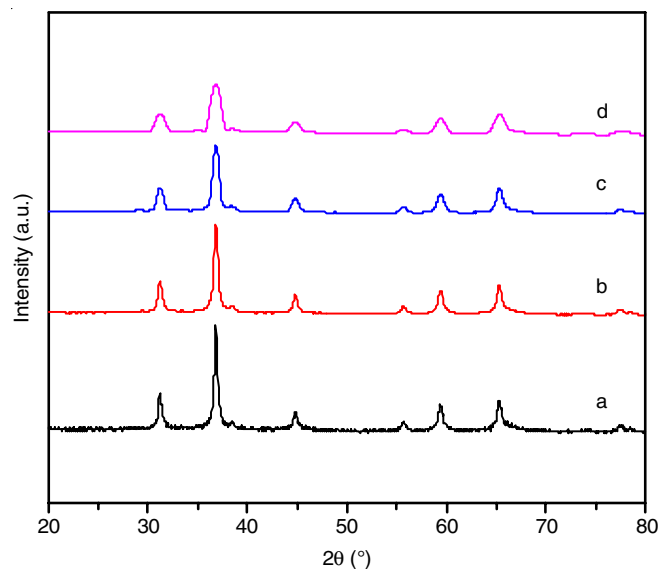


Fig. 1. XRD pattern (a) Mn_3O_4 (b-d) Nd-doped Mn_3O_4 (0.01, 0.02 and 0.03) samples

Morphology analysis: The surface morphology analysis images were exploited to examine the morphology and structure for proportion Nd doped Mn_3O_4 ($x = 0.01, 0.02$ and 0.03). The SEM images of undoped Mn_3O_4 and Nd doped Mn_3O_4 nanopowders are presented in Fig. 2a-d. The materials show grain morphology. Most of the grains tend to be a shape of hexagonal. Images shows nano-microparticles are homogeneous and have irregular shape. Agglomeration takes place among the particles, which might be as a consequence of interaction of dipole-dipole between the particles. The as-synthesized materials grain size is measured by employing a method of line intercepts that usually situated in the middle of 15 and 22 nm. By increasing the concentration of Nd, the particle size increases [20].

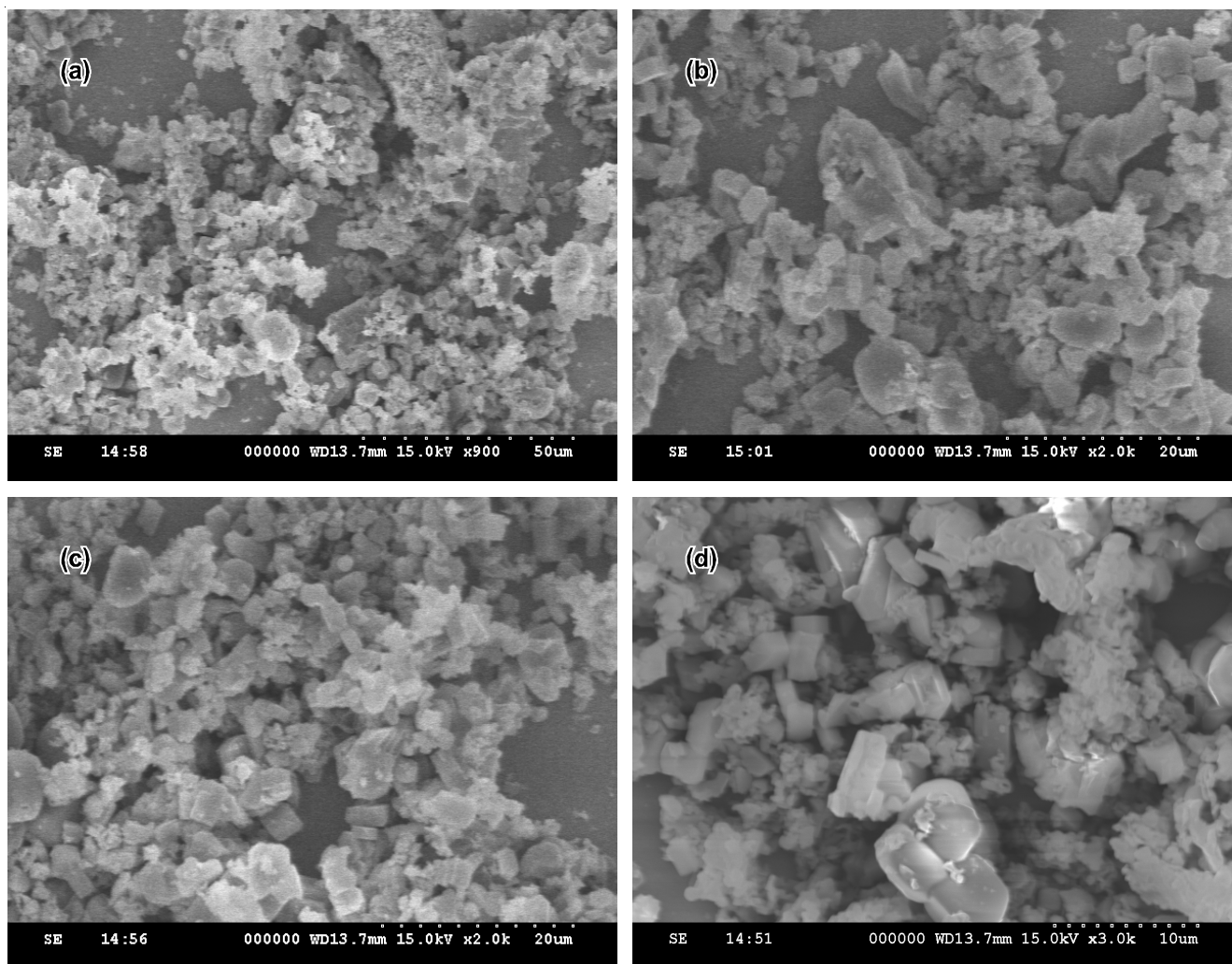


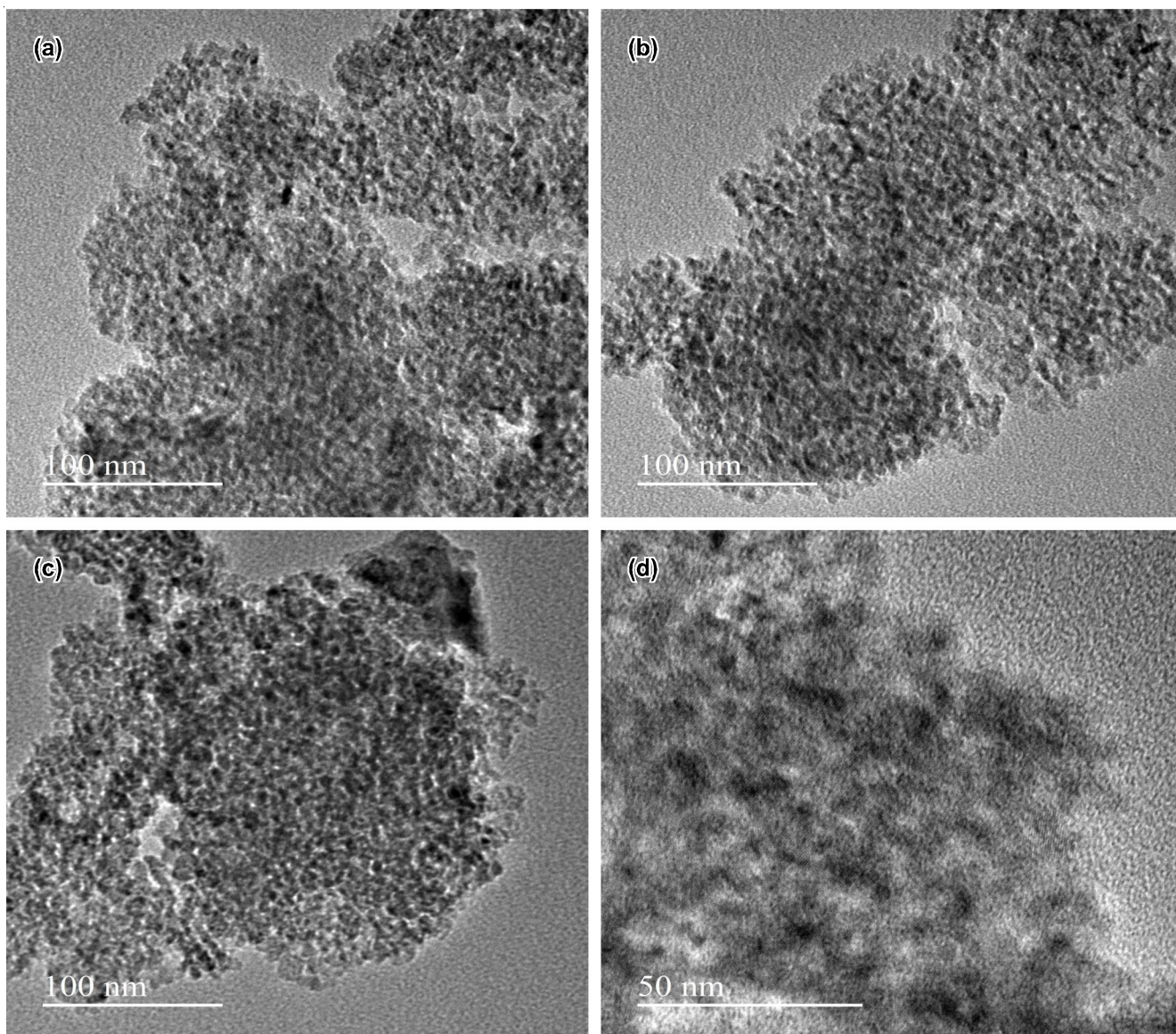
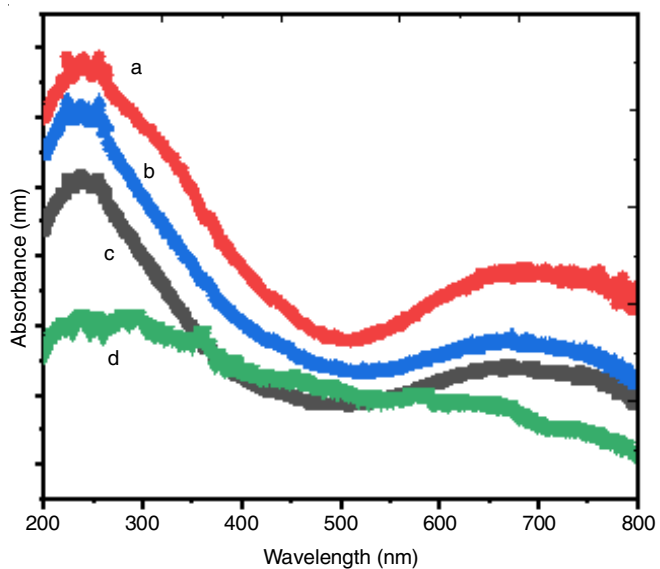
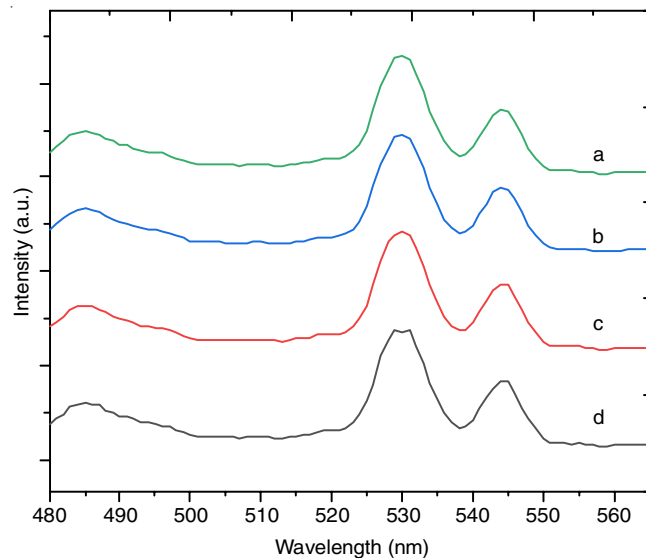
Fig. 2. SEM surface morphology for Nd-doped Mn_3O_4 samples

The corresponding TEM images of Nd doped Mn_3O_4 (0.01, 0.02, and 0.03) are shown in Fig. 3a-d. From TEM images, a consistent particles distribution is observed, which have a distinguishable boundaries on grain. The particles get agglomerated similar to a chain and also every particle displays a structure of ball shaped granular. In fact, it is somewhat complicated in finding the particles accurate size from the TEM photographs. Increase in Nd doping ratio from 0.01 to 0.02 % resulted the aggregation of larger particles (Fig. 3).

Diffuse reflectance spectroscopic studies (DRS): Nd-doped Mn_3O_4 materials diffuse reflectance UV-visible spectrophotometry has been recorded wavelength region starting from 350 to 800 nm. Barium sulphate (spectroscopic grade) was chosen being a reference. For Nd doped Mn_3O_4 materials, a wide shoulder noticed through the region of wavelength 350-375 nm is most likely due to the some structural defect (Fig. 4). The shoulder peak intensity decreases, if Nd content is increased indicating the minimization of growth of crystallite as well as structural defects because of effective microwave method. A blue shift which is comparable has been noticed related to corresponding band gap in a variety of semiconducting material since, the optical properties highly be dependent on the particle dimensions. Hence, particle-size distribution is likely to be a reason in optical spectra homogeneous broadening [21,22].

Photoluminescence analysis: Photoluminescence spectra provide direct details in relation to the existence of defects in metal oxide samples. A 325 nm wavelength of xenon lamp is applied for being an excitation source to get photoluminescence spectrum. But, in present work, a blue along with green PL emission bands at 450 and 540 nm, respectively in the visible region for Nd doped Mn_3O_4 nanoparticles were observed (Fig. 5). The metal atoms which are doped alter the Nd atom coordination environment and adjust the Mn_3O_4 electronic structure through introducing localized energy levels of electrons in atoms on the photoluminescence emission bands.

Generally, Nd doped Mn_3O_4 emits ultraviolet, green, blue and violet emissions. The emission of ultraviolet referred to as near band-edge emission is due to recombination of electron/hole pair from free excitations. The emission of violet arises by the defect centers, for instance, interstitials of O, Nd and Mn. Likewise, emission of blue originates from the O and Mn ions transition of charge-transfer from by the lattices of Mn_3O_4 . The emission of green is caused by many structural defects existing on the synthesized materials. The more substantial ratio of surface-area to volume could create interstitials and vacancies (surface-defects) in higher density that can generate a level of traps as well as the reason for visible emission [23-25].

Fig. 3. TEM images for Nd-doped Mn_3O_4 samplesFig. 4. Diffused reflectance UV-visible spectra of and Nd-doped Mn_3O_4 samplesFig. 5. Photoluminescence spectra for Nd-doped Mn_3O_4 samples (exc. wavelength 345 nm)

Vibrating sample measurements (VSM): The magnetic qualities for Nd doped Mn₃O₄ were measured using VSM vibrating sample magnetometer at room temperature around on applied field extending effective towards ± 10 kOe, which evidently designates that the products are split from the liquid from the entry for outside field that is magnetic. Present work, magnetic hysteresis (M-H) loop demonstrate on the samples need ferromagnetic properties within magnetic nature (Fig. 6). Hysteresis ethics, such as, remanant magnetization (M_r), saturation magnetization (M_s) and coercivity (H_c) and the structural morphology of the products depends on the type of exploited precursor [26,27].

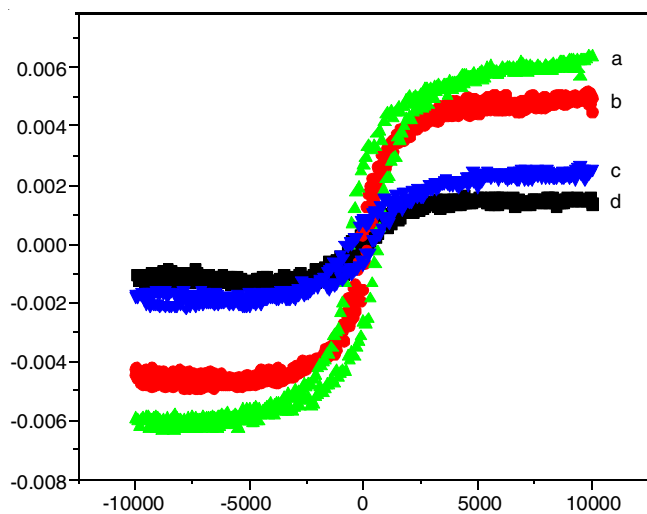


Fig. 6. Magnetic hysteresis loops of Nd-doped Mn₃O₄ samples

The changes in magnetic hysteresis loop could possibly be described by reason of magnetic contribution based on the strong exchange interaction orientation at s-f couple by Nd(III) ions. Increasing the concentration of Nd results in increase the magnetization linear behaviour value. Evidently, oxygen vacancies concentration played a significant role in mediating the interaction of ferromagnetic exchange amongst Nd³⁺ ions. The current results have shown that interstitials and oxygen vacancies were created by increasing doping concentration of Nd³⁺ which can be accountable with regards to observed long range ferromagnetism. Furthermore, rare earth ions holes or electrons could intermediate the ferromagnetism because of s-f coupling amongst rare earth ions. This may be attributable to uncompensated spins ferromagnetic arrangement on the samples surface. The Nd³⁺ states existence could possibly be the reason for weak ferromagnetism at room temperature.

Specific surface area: The specific surface area was obtained by using BET equation to measure the adsorbed N₂ on Nd doped Mn₃O₄. The average micropore diameter was obtained by H-K method [28] and the total pore volume and micropore volume was attained by t-plot. The specific surface area (S_{BET}) together with the pore radius (R_p) and pore volume (V_p) and crystallite size (nm) of Nd doped Mn₃O₄ samples are presented in Table-1. This implies that the surface structure of activated catalysts are very similar and the activity differences are just due to the higher surface area of Nd doped Mn₃O₄ samples having more number of active sites per unit mass of the catalyst. In general, comparing these values with the agglomerate distribution values, it is found that very fine particles have a tendency

TABLE-1
BET SURFACE AREA, AVERAGE PORE DIAMETER, PORE VOLUME AND THEIR CRYSTALLITE SIZE (nm) OF Nd DOPING Mn₃O₄ PREPARED BY THE CM AND MM

Catalyst	S_{BET} (m ² /g)	R_p (Å)	V_p (cm ³ /g)	Crystallite size (nm) from XRD
A	62.59	26.12	0.1123	23.89
B	68.90	23.34	0.1307	21.75
C	73.59	22.65	0.1077	20.12
D	84.90	15.53	0.1289	19.56

to react with each other, reducing the high surface energy and forming agglomerates of nanostructures. Generally, the specific surface area of a material is attributed to both the external surface of particles and the internal surface of pores, if the material is porous. This relatively high specific surface area of Nd doped Mn₃O₄ samples is beneficial to their catalytic activity.

Catalytic studies: Nd-doped Mn₃O₄ catalytic performance were studied by evaluating its application in the selective benzyl alcohol oxidation into benzaldehyde by using acetonitrile as solvent and H₂O₂ as oxidant. Usually, benzyl alcohol oxidized directly into benzaldehyde, subsequently oxidized into benzoic acid as well as benzyl benzoate. Though, in the present case exclusively benzaldehyde was recognized being an oxidation product. Since, the selective oxidation is aim of the present study. Blank reaction performed over Nd doped Mn₃O₄ according to the similar reaction conditions displayed minimal benzaldehyde yields. In a controlled experiment, benzaldehyde yield was just 3.2 % in the absence of oxidant and catalyst.

In absence of oxidant, Nd doped Mn₃O₄ showed only 6.9 % yield of benzaldehyde and in absence of catalyst, no significant amount of benzaldehyde was produced which indicated that H₂O₂ alone is unable to oxidize benzyl alcohol into benzaldehyde. In order to increase the yield of benzaldehyde, several promoters, such as, Nd doped Mn₃O₄, H₂O₂ and solvent were added. Among the three additives, H₂O₂ was the most effective promoter to achieve higher yield of benzaldehyde. The oxidation of alcohols plays an important role in organic synthesis, while the development of new oxidative processes continues drawing attention inspite of the availability of numerous oxidizing reagents. Hence, in terms of economic and environmental concern, catalytic oxidation processes with low cost and environmental oxidants are extremely valuable. In the present study, a maximum yield of 94.1 % of benzaldehyde is obtained in H₂O₂ medium using Nd 0.03 % doped Mn₃O₄ catalyst (Table-2).

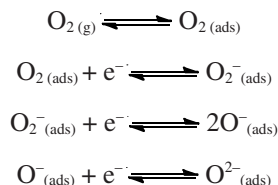
TABLE-2
CATALYTIC ACTIVITY OF Nd (0.01, 0.02 AND 0.03) DOPING Mn₃O₄ CATALYSTS CATALYST IN THE PRESENCE OF H₂O₂ OXIDANT FOR BENZYL ALCOHOL TO BENZALDEHYDE OXIDATION

Entry	Catalyst	Oxidant	Yield (%)
1	Without catalyst	Without oxidant	03.2
2	With catalyst	Without oxidant	06.9
3	Without catalyst	With oxidant	22.1
4	A	H ₂ O ₂	61.5
5	B	H ₂ O ₂	66.9
6	C	H ₂ O ₂	70.3
7	D	H ₂ O ₂	91.8

Reaction conditions: Catalyst 0.5 g, benzyl alcohol, 5 mmol, acetonitrile, 5 mmol, H₂O₂, 5 mmol, reaction temperature, 80 °C and reaction time 8 h.

Mechanism: With a purpose to discover mechanism towards oxidation of benzyl alcohol using Nd doped Mn_3O_4 , thermoelectric power (TEP) study was performed and as a consequence, it appears that Nd doped Mn_3O_4 is a p-type semiconductor, in which electrons are considered as the most important charge carriers in thermoelectric power [29].

The oxygen molecules in atmosphere are adsorbed on the Nd doped Mn_3O_4 surface by means of O^{2-} and O^- , therefore the conduction electrons decreases. The O^- adsorption is extremely responsive at 100 °C and as a consequence will make the material more responsive to the existence of reducing gas [30,31].



The reaction among the oxygen species is ionic and the reducing alcohol produces water and aldehyde [32].



The moment when the vapours of alcohol enters into exposure, the oxygen ions on the surface of oxide reacts quite possibly with O^{2-} and O^- ions and as a consequence becomes oxidized into water and aldehyde, with the liberation of electron. Desorption of aldehyde molecules (weakly bound) coming from the oxide surface produces newer vacant sites intended for the forthcoming molecules of alcohol [33-35] and for that reason the activity of catalyst is enhanced.

Conclusion

Neodymium doped Mn_3O_4 (0.01, 0.02 and 0.03 %) hexagonal like nanopowders are synthesized by using microwave method and then its optical, structural and the magnetic properties were studied. The results indicated that Nd doped Mn_3O_4 is highly active towards the selective oxidation of benzyl alcohol to benzaldehyde at a low temperature with very high yield, due to the presence of more number of active sites.

CONFLICT OF INTEREST

The authors declare that there is no conflict of interests regarding the publication of this article.

REFERENCES

- D.-C. Liang, Q. An, P. Jin, X.-K. Li, H. Wei, J. Wu and Z.-G. Wang, *Chin. Phys. B*, **20**, 108503 (2011); <https://doi.org/10.1088/1674-1056/20/10/108503>.
- K.E. Sickafus, J.M. Wills and N.W. Grimes, *J. Am. Ceram. Soc.*, **82**, 3279 (1999); <https://doi.org/10.1111/j.1151-2916.1999.tb02241.x>.
- D. Bahadur and S. Rajakumar, *J. Chem. Sci.*, **118**, 15 (2006); <https://doi.org/10.1007/BF02708761>.
- F. Gözüak, Y. Köseoglu, A. Baykal and H. Kavas, *J. Magn. Magn. Mater.*, **321**, 2170 (2009); <https://doi.org/10.1016/j.jmmm.2009.01.008>.
- Y. Koseoglu, F. Alan, M. Tan, R. Yilgin and M. Ozturk, *Ceram. Int.*, **38**, 3625 (2012); <https://doi.org/10.1016/j.ceramint.2012.01.001>.
- Y. Chen, L. Yang, C. Feng and L.-P. Wen, *Biochem. Biophys. Res. Commun.*, **337**, 52 (2005); <https://doi.org/10.1016/j.bbrc.2005.09.018>.
- I. Kostova, R. Kostova, G. Momekov, N. Trendafilova and M. Karaivanova, *J. Trace Elem. Med. Biol.*, **18**, 219 (2005); <https://doi.org/10.1016/j.jtemb.2005.01.002>.
- H. Yang, L. Guo, W. Yan and H. Liu *J. Power Sources*, **159** 1305 (2006); <https://doi.org/10.1016/j.jpowsour.2005.11.106>.
- C. Ragupathi, S. Narayanan, M.P. Pachamuthu, N.M. Basith, R. Kannapiran and G. Ramalingam, *Adv. Sci. Eng. Med.*, **10**, 882 (2018); <https://doi.org/10.1166/asem.2018.2188>.
- W. Qin, L. Xu, J. Song, R. Xing and H. Song, *Sens. Actuators B Chem.*, **185**, 231 (2013); <https://doi.org/10.1016/j.snb.2013.05.001>.
- P. Gunawan, L. Mei, J. Teo, J. Ma, J. Highfield, Q. Li and Z. Zhong, *Langmuir*, **28**, 14090 (2012); <https://doi.org/10.1021/la302590g>.
- C. Ragupathi, J.J. Vijaya, R.T. Kumar and L.J. Kennedy, *J. Mol. Struct.*, **1079**, 182 (2015); <https://doi.org/10.1016/j.molstruc.2014.09.045>.
- X. Fu, L.A. Clark, Q. Yang and M.A. Anderson, *Environ. Sci. Technol.*, **30**, 647 (1996); <https://doi.org/10.1021/es950391v>.
- F. Cheng, Z. Peng, C. Liao, Z. Xu, S. Gao, C. Yan, D. Wang and J. Wang, *Solid State Commun.*, **107**, 471 (1998); [https://doi.org/10.1016/S0038-1098\(98\)00265-8](https://doi.org/10.1016/S0038-1098(98)00265-8).
- M. Sajjia, M. Oubaha, M. Hasanuzzaman and A.G. Olabi, *Ceram. Int.*, **40**, 1147 (2014); <https://doi.org/10.1016/j.ceramint.2013.06.116>.
- M. Sales, C. Valentín and J. Alarcón, *J. Eur. Ceram. Soc.*, **17**, 41 (1997); [https://doi.org/10.1016/S0955-2219\(96\)00069-6](https://doi.org/10.1016/S0955-2219(96)00069-6).
- M.H. Mahmoud, A.M. Elshahawy, S.A. Makhlof and H.H. Hamdeh, *J. Magn. Magn. Mater.*, **343**, 21 (2013); <https://doi.org/10.1016/j.jmmm.2013.04.064>.
- I. Khan, S. Khan, H. Ahmed and R. Nongjai, *AIP Conf. Proc.*, **1536**, 241 (2013); <https://doi.org/10.1063/1.4810190>.
- G. Williamson and R. Smallman, *Philos. Mag.*, **1**, 34 (1956); <https://doi.org/10.1080/14786435608238074>.
- L. Li, C. Xiang, X. Liang and B. Hao, *Synth. Met.*, **160**, 28 (2010); <https://doi.org/10.1016/j.synthmet.2009.09.026>.
- C.H. Ong and H. Gong, *Thin Solid Films*, **445**, 299 (2003); [https://doi.org/10.1016/S0040-6090\(03\)01175-1](https://doi.org/10.1016/S0040-6090(03)01175-1).
- Y.C. Ng and M. Shamsuddin, *J. Iran. Chem. Soc.*, **8(S1)**, S28 (2011); <https://doi.org/10.1007/BF03254279>.
- C. Ragupathi, J.J. Vijaya, L.J. Kennedy and M. Bououdina, *Ceram. Int.*, **40**, 13067 (2014); <https://doi.org/10.1016/j.ceramint.2014.05.003>.
- C. Ragupathi, J.J. Vijaya and L.J. Kennedy, *Mater. Sci. Eng. B*, **184**, 18 (2014); <https://doi.org/10.1016/j.mseb.2014.01.010>.
- C. Ragupathi, J.J. Vijaya, L.J. Kennedy and M. Bououdina, *Mater. Sci. Semicond. Process.*, **24**, 146 (2014); <https://doi.org/10.1016/j.mssp.2014.03.026>.
- Y. Ichiyanagi, Y. Kimishima and S. Yamada, *J. Magn. Magn. Mater.*, **272-276**, E1245 (2004); <https://doi.org/10.1016/j.jmmm.2003.12.377>.
- A.S. Bhatt, D.K. Bhat, C. Tai and M.S. Santosh, *Mater. Chem. Phys.*, **125**, 347 (2011); <https://doi.org/10.1016/j.matchemphys.2010.11.003>.
- S.K. Nataraj, B.H. Kim, J.H. Yun, D.H. Lee, T.M. Aminabhavi and K.S. Yang, *Mater. Sci. Eng. B*, **162**, 75 (2009); <https://doi.org/10.1016/j.mseb.2009.03.008>.
- T. Selvamani, A. Sinhamahapatra, D. Bhattacharjya and I. Mukhopadhyay, *Mater. Chem. Phys.*, **129**, 853 (2011); <https://doi.org/10.1016/j.matchemphys.2011.05.055>.
- J.P. Muñoz Mendoza, O.E. Ayala Valenzuela, V. Corral Flores, J. Matutes Aquino and S.D. De la Torre, *J. Alloys Compd.*, **369**, 144 (2005); <https://doi.org/10.1016/j.jallcom.2003.09.075>.
- N. Yamazoe and N. Miura, *Chemical Sensor Technology*, 4th edition, Elsevier, Amsterdam, edn 4, p. 19 (1992).
- L. Promsong and M. Sriyudthsak, *Sens. Actuators B Chem.*, **25**, 504 (1995); [https://doi.org/10.1016/0925-4005\(95\)85108-9](https://doi.org/10.1016/0925-4005(95)85108-9).
- M.R. Islam, N. Kumazawa and M. Takeuchi, *Appl. Surf. Sci.*, **142**, 262 (1999); [https://doi.org/10.1016/S0169-4332\(98\)00712-0](https://doi.org/10.1016/S0169-4332(98)00712-0).
- P. Song, J. Hu, H. Qin, L. Zhang and K. An, *Mater. Lett.*, **58**, 2610 (2004); <https://doi.org/10.1016/j.matlet.2004.03.028>.
- S. Komarneni, R. Roy and Q.H. Li, *Mater. Res. Bull.*, **27**, 1393 (1992); [https://doi.org/10.1016/0025-5408\(92\)90004-J](https://doi.org/10.1016/0025-5408(92)90004-J).